Monitoring of Backside Weld Bead Width from High Dynamic Range Images Using CNN Network

Rui Yu, Joseph Kershaw, Peng Wang, Senior Member, IEEE, and YuMing Zhang*, Senior Member, IEEE

Abstract— Weld penetration determines the integrity of the weld produced and must be controlled in automated welding. Due to the dramatic development of the neural networks, research has been done to use convolutional neural network (CNN) as a deeplearning model to automatically extract weld pool features from the weld pool image. However, for the deep learning to be effective, the raw information must contain such feature that correlate to the weld penetration. High dynamic range (HDR) cameras provide an effective to image the weld pool scene without being overshaded by the arc so that the rich information from the weld pool may be preserved. Unfortunately, limited studies have been done to extract possible rich information in HDR images and use the extracted relevant information/features to predict what are occurring underneath the work-piece, in particular when the weld pool is subject to dynamic change as during its feedback control. In this work, an HDR camera is used to capture the weld pool image from the topside. What occurs at the same time underneath the work-piece is captured by another camera aiming at the back-side surface of the weld pool forming the ground truth for training. A CNN network model is proposed to extract the relevant information from the rich information source/HDR top-side image and map to the label representing what occurs underneath the work-piece. To train the network, a series of experiments have been conducted with welding current and speed to change randomly, generating various weld pool images and backside bead widths/images in order to ensure the reliability and robustness of the trained network in a varying environment. With the analysis of the result, it is verified that the well-trained CNN network could improve the prediction result of the backside bead width.

I. INTRODUCTION

When two pieces of metals are joined, a heat source is applied to melt their interface. Upon the solidification of the melted metal, the two surfaces of the interface from two pieces of metals are joined. The depth of weld penetration refers to how deeply the interface has been melted from the heating surface and the width of the back-side weld bead refers to how wide the metals around the interface has been melted on the opposite side of the heating surface if the entire thickness of the work-piece has been melted. They are both referred to as weld penetration, former for partial penetration and latter for full penetration. This work concerns accurate monitoring of the latter. It is important as it determines the weld integrity and is required by manufacturers.

It is apparent that what is to be monitored is not visible from

the heating side where a robot can conveniently carry a sensor. We have to sense phenomena occurring on the heating side and then derive what occurs underneath. The most promising phenomena may be visual as a human welder can make quality weld by observing the weld pool while there are also other approaches [1]–[8]. However, the bright arc makes its visual observation challenging. A camera without special filter or other special techniques would result in an image as shown in Fig. 1.

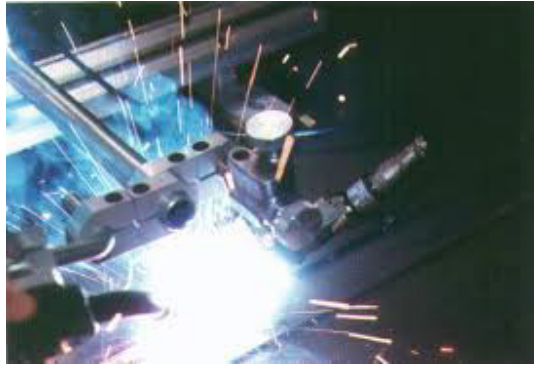


Fig. 1. A view of arc welding process using a standard camera from open source on the internet.

To image the weld pool clearly, studies have been carried to image the weld pool area when the arc is extinguished [9], [10], which periodically occurs during short-circuiting transfer in gas metal arc welding (GMAW), or when the arc current is at the low, base level so that the arc brightness weakens [11], [12]. Denoising techniques have also been studied, either filtering raw images [13], [14] or inpainting images from strong process interferences [15]. To clearly image the weld pool in the presence of a bright arc, a pulse laser was also projected to the weld pool area and the camera shutter was synchronized with this pulse with the peak power in nanoseconds [6], [16]. For an illumination laser with milliwatt power, the peak power increased to tens of kilowatts. The laser became much brighter than the arc when the camera opened the shutter to image. As a result, clear weld pool images were acquired. However, the equipment is complex and a passive vision without an illumination laser is often preferred [17]. Recently, HDR cameras have been developed where the brightness is not proportional to the incident

<u>yuming.zhang@uky.edu</u>). This work is partially funded by the University of Kentucky and the National Science Foundation under grant # No. 2024614.

radiation received but to its logarithm [18], [19]. As such, are and weld pool can both be imaged without the weld pool be overshaded by the arc[20], [21]. As HDR cameras have been commercialized for welding applications, methods to effectively extract useful information should be developed.

HDR cameras have made views close to that of human available to machines. It becomes interesting if useful welding process information, in particular the back-side bead width that is most challenging for welding robots to assure, can be effectively extracted from such views/images. Conventionally, features are proposed through hand-craft engineering approach from weld pool images and correlated to the welding process state to be monitored [16], [22] and this has been the case also for HDR images [21]. However, such a method may also not guarantee the hidden information be successfully extracted, while deep-learning networks that automatically extract hidden information may if the information is indeed contained [23]-[25]. Unfortunately, deep-learning models have not been adequately used to take advantage of the rich information in HDR images except for in [26] that used a CNN model to process HDR images for laser bed additive manufacturing where the most concerned arc is absent, and for in [27] that used an image segmentation network to process HDR images in order to obtain a clear weld pool boundary.

This study aims at predicting the backside bead width from an HDR image using a CNN, that is known, and has been demonstrated [28]–[31], as a suitable deep-learning model to automatically extract information from images. The training data were collected from designed experiments by imaging the weld pool from both the top and back surfaces. The top weld pool image was directly fed into the network after simple cropping while the bottom bead image was processed by a specific algorithm to obtain the training ground truth.

II. SYSTEM AND EXPERIMENTS

A. Experimental System

The experimental set-up used is shown in Fig. 2 (a). It has a welding, sensing, control and motion subsystem. The welding subsystem performs the gas tungsten arc welding (GTAW) using a Miller Maxstar 210 welding power source and a welding torch with a tungsten electrode of diameter 2.4 mm with pure argon at 99.99% purity as the shield gas. The sensing subsystem includes one Point Grey camera FL3-FW-03S1C to capture images from the back surface of the workpiece vertically and an HDR camera Xiris XVC-1100 to capture the top images of the weld pool at 60° angle with the torch from the leading position. After the backside images are captured, they will be binarized using a threshold to produce the labels and then paired with the topside images captured at the same time to build the dataset. In the motion subsystem, the workpiece was driven by a step motor to move in one direction on a rail and the motion was controlled in real time to change the travel speed. All these subsystems are controlled by a computer using a PCI-6229 National Instruments data acquisition card, which works and operates

in the C++ environment to control the welding current and the time and speed to move the workpiece, and to operate the cameras to capture the weld pool images from both sides. Fig. 3 shows example images captured, with (a) and (b) the original images and (c) the processed backside image using a pre-set threshold that will be detailed later.

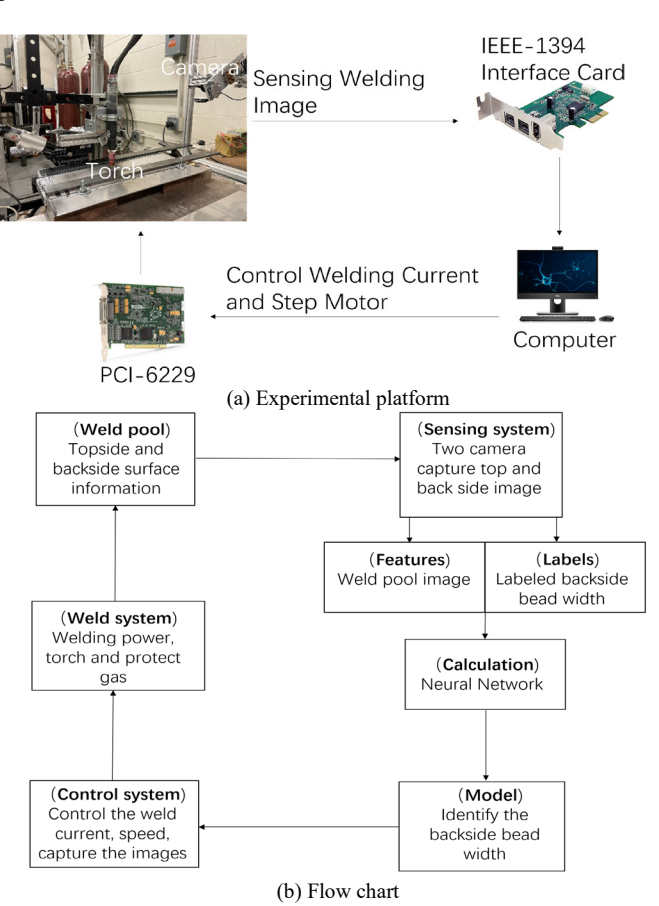


Fig. 2. Platform and Flow chart of the experiment system

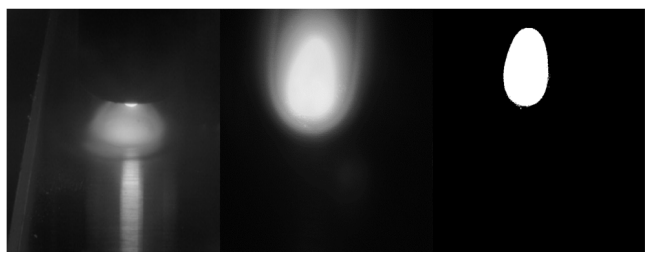


Fig. 3. Captured and processed images. From left to right: topside image, backside image, and threshold backside image.

B. Procedure

Fig. 2(b) illustrates the experimental process. When the welding process starts, the welding power source and the motion system will both receive a signal from the control system to determine the current waveform and the travel speed. During the welding process, the welding current and the workpiece travel speed vary randomly between 90 A to 130 A and 1.4 mm/s to 2 mm/s every 2 seconds respectively to simulate dynamic environment under different heat input (Fig. 4) as typical during control. After the current is applied, the input heat will start to melt the workpiece. The weld pool

begins to form and then grow as the input heat accumulates. Within a few seconds, the weld pool will penetrate the workpiece from the heating (top) to the opposite (back-side) surface forming a fully penetrated weld pool. The topside and backside cameras monitor this process and capture images from both sides of the weld pool simultaneously. The captured topside images are the inputs of the CNN model and the backside images are used to generate the labels. During the training process, the captured topside image will be paired with the label captured at the same time from the backside. The paired images were divided into three datasets to train, validate, and test the CNN model respectively.

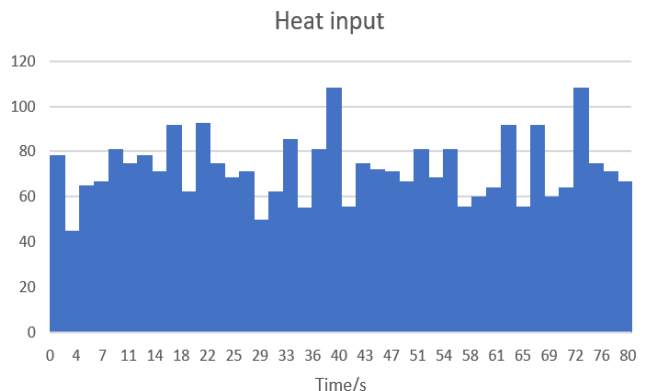


Fig. 4. Heat input

C. Data Collection

With the welding parameters listed in Table I, six experiments have been designed and conducted using GTAW process and totally 28560 image pairs have been collected. The parameters of the cameras such as the frame rate, sharpness, gamma, shutter, and gain are listed in Table II for both cameras. The material used to conduct the experiments is stainless steel 304L.

TABLE I. WELDING PARAMETERS

Material	Thickness	Arc Length	Gas Flow Rate
Stainless Steel 304 L	1.85 (mm)	4.8 (mm)	7 (L/min)

TABLE II. CAMERA PARAMETERS

Camera	Sharpness	Gamma	Shutter Speed	Frame Rate	Gain
Тор	3000	2.0	5 (ms)	60 (fps)	10 dB
Bottom	3000	2.5	0.2 (ms)	60 (fps)	0 dB

As shown in Fig. 5 and Fig. 6, with the random welding current and welding speed, the heat input, i.e., IU/v where I,U, and v are the welding current, arc voltage and travel/welding speed respectively, at different time will be different during the welding process. (The arc voltage is generally considered a constant and does not change with the welding current and

travel speed.) Therefore, different welding and arc conditions will be generated, as well as different state of the weld pool and backside bead width. Successful training and testing with this various state under dynamic change will make sure that the developed network has the needed reliability and robustness.

To label the weld pool backside width, there were some previous methods introduced on how to convert image to the bead width value [32]. However, it was designed for spot welding where the arc is stationary and the resultant weld pool is round. In this work, the arc/torch moves in relation to the work-piece so that the weld pool becomes tear-drop shaped. To contest this issue, we developed an improved version from the previous ones [32].

First, the backside image will be binarized into black and white to make sure the pool area distinct from the surrounding area. All contours in the binarized image were then detected and the contour with the largest area was used as the pool contour. The widths from all the rows in this contour were then counted, and the average of the top ten widths was calculated as the width of the back-side bead. The width in pixels can be converted to millimeters through calibration. The threshold in the binarized process was decided iteratively. An arbitrary value was first tried and the backside image was then processed. The binarized image was then compared with the actual back bead on the work-piece to check if it matched the trend. If binarized images showed full penetration but the work-piece did not, the threshold was then increased and vice versa. The finally chosen threshold was set at 172. The conversion ratio 0.06 mm/pixel was obtained through a calibration by comparing the image reading and actual size of a given shape.

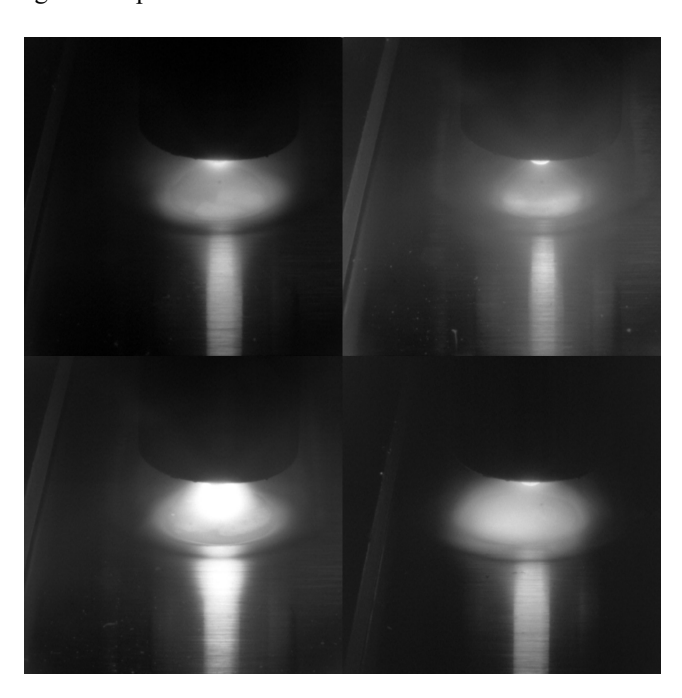


Fig. 5. Weld pool at different state

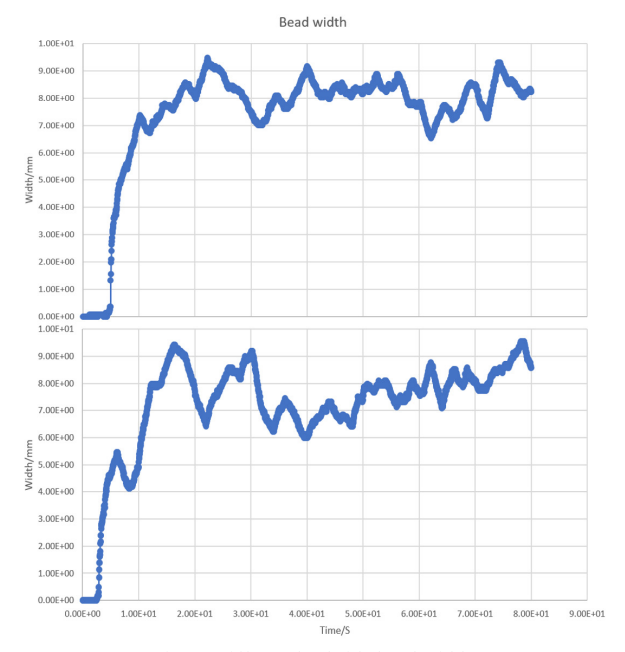


Fig. 6. Different backside bead width

III. NETWORK MODEL

Network's performance and reliability are significantly influenced by its structure. After several attempts, the network architecture shown in Fig. 7 was chosen. The details are given in Table III. The input image of the network is fed into a typical convolution layer followed by a pooling layer. This convolution and pooling process repeats 4 times, with the parameters of convolution layers as (1, 32, 5, 2, 2), (32, 64, 3, 2, 1), (64, 128, 3, 2, 1), (128, 256, 3, 2, 1) respectively. Batch normalization and ReLU activation were performed between each convolution and pooling layer. After the four convolution-pooling processes, the input image will be represented as a 1 by 256 feature vector. The feature vector will then be processed by two fully connected layers to predict the backside bead width.

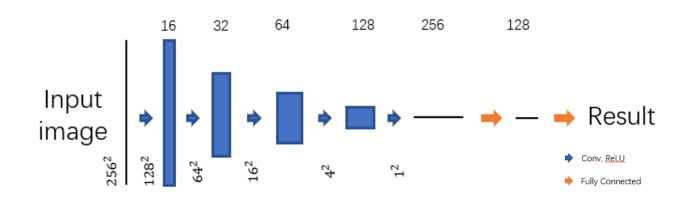


Fig. 7. CNN architecture.

TABLE III. CNN CONFIGURATION

Layer Name	Feature Map Size	Kernel Size	Stride	Padding
Input	256 * 256 * 1	-	-	-
Conv 1	128 * 128 * 32	5	2	2
MaxPool	64 * 64 * 32	2	-	-
Conv 2	32 * 32 * 64	3	2	1
MaxPool	16 * 16 * 64	2	=	-

Conv 3	8 * 8 * 128	3	2	1
MaxPool	4 * 4 * 128	2	-	-
Conv 4	2 * 2 * 256	3	2	1
MaxPool	1 * 1 * 256	2	-	-
FC 1	256	-	-	-
FC 2	128	-	-	-
Output	1	-	-	-

With such a network architecture, we gradually reduce the feature's size but increase the channel.

IV. TRAINING AND RESULTS

We used a NVIDIA GTX 2080 to conduct the training and validation for 100 iterations having Pytorch library implementation under Python environment.

With all the 28560 image pairs in our dataset, we divided them into three datasets for training, validation and testing with sizes of 19040, 4760 and 4760 respectively. The network was trained using an SGD optimizer with mean-square error loss, learning rate of 0.0001 and batch size of 16. The learning rate and batch size were decided from the best performance model which was obtained through multiple trainings with different learning rate as 0.01, 0.001, 0.0001 and different batch size as 16, 32, 64. The training and validation loss over 100 epochs are shown in Fig. 8. The model achieved its lowest validation loss at epoch 41.

The model at the epoch 41 was thus selected to predict the test data. The result is shown in Fig. 9. Comparing the predicted with the ground truth label, it is obvious that the model is able to strongly correlate the topside HDR weld pool image with the backside bead width. The model did not perform well when the welding starts. This was probably because, before the welding starts, all the images captured were pure dark and significantly differ from images captured during welding. In addition, the pure dark images in the dataset are too small for the model to correlate to the labels. It is also obvious that, when the width experiences drastic changes the prediction lags behand. This is because the change in the current/heat input first directly reflects on the topside weld pool surface/image where it is imposed but takes time for it to transfer to the backside.

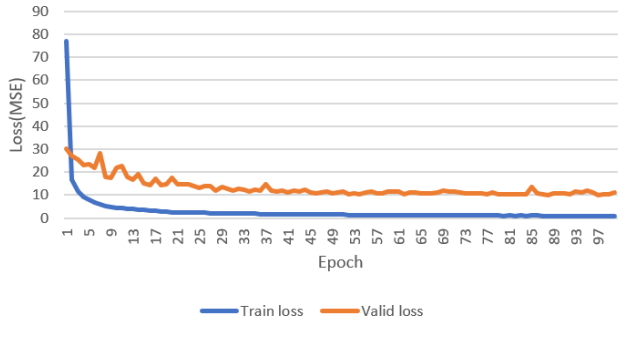


Fig. 8. Model training curve

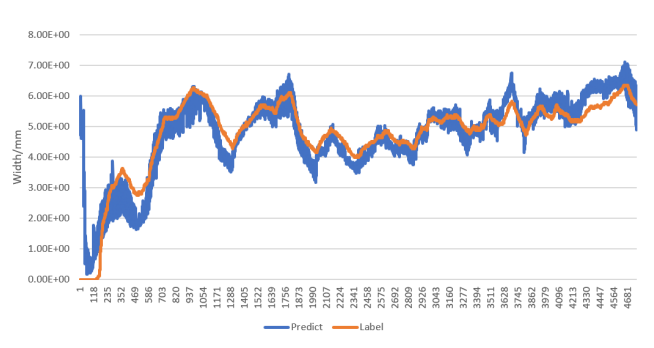


Fig. 9. Performance on test data

V.CONCLUSION AND FUTURE WORK

This paper developed an effective approach to monitor the backside width of the weld bead from a topside weld pool image that can be conveniently obtained using a camera attached to the welding torch. The use of an HDR camera enables imaging the weld pool without being overshaded by the arc overwhelmingly. The resultant images contain complete, visual information about the process although it is complex and still noisy. However, while HDR imaging provides an effective method to preserve the rich information in the weld pool, it is not clear and straightforward what is crucial in the image that determines the backside bead width. While an active vision approach can see some features more clearly, some other features may have been lost unintentionally. A CNN model allows automatically extracting relevant crucial features from complex images/scenes. It has been shown that a carefully designed CNN model is capable of extracting the right information/features from the HDR images to strongly correlate them to what occur underneath the work-piece as represented by the backside bead width in this study.

REFERENCES

- [1] D. J. Kotecki, D. L. Cheever, and D. G. Howden, "Mechanism of Ripple Formation During Weld Solidification Ripples on GTA spot welds are explained by pool sur-face oscillations during solidification, as seen by high speed motion pictures".
- [2] Y. H. Xiao and G. den Ouden, "Weld Pool Oscillation during GTA Welding of Mild Steel The oscillation behavior of the GTA weld pool depends on the welding conditions and can be used for inprocess control of weld penetration".
- [3] Y. H. Xiao and G. den Ouden, "A Study of GTA Weld Pool Oscillation Monitoring oscillation frequency in the weld pool may offer a means of controlling joint penetration".
- [4] L. A. Lott, J. A. Johnson, and H. B. Smartt, "Real-time ultrasonic sensing of arc welding processes," Jan. 1983, doi: 10.2172/6810314.
- [5] R. FENN, "ULTRASONIC MONITORING AND CONTROL DURING ARC FUSION WELDING," http://dx.doi.org/10.1080/10589758508952913, vol.

- 2, no. 2, pp. 43–53, Jun. 2007, doi: 10.1080/10589758508952913.
- [6] Y. CHENG, Q. WANG, W. JIAO, J. XIAO, S. CHEN, and Y. ZHANG, "Automated Recognition of Weld Pool Characteristics from Active Vision Sensing," *Welding Journal*, vol. 100, no. 5, May 2021, doi: 10.29391/2021.100.015.
- [7] Y. M. Zhang, L. Li, and R. Kovacevic, "Dynamic Estimation of Full Penetration Using Geometry of Adjacent Weld Pools," *Journal of Manufacturing Science and Engineering*, vol. 119, no. 4A, pp. 631–643, Nov. 1997, doi: 10.1115/1.2831197.
- [8] "US9604301B2 Method to monitor and control weld penetration in gas tungsten welding and full-position pipe welding Google Patents." https://patents.google.com/patent/US9604301 (accessed Feb. 20, 2022).
- [9] J. Huang, W. Pan, J. Chen, Y. Shao, M. Yang, and Y. Zhang, "The transient behaviours of free surface in a fully penetrated weld pool in gas tungsten arc welding," *Journal of Manufacturing Processes*, vol. 36, pp. 405–416, Dec. 2018, doi: 10.1016/J.JMAPRO.2018.10.024.
- [10] K. Yamazaki *et al.*, "Measurement of surface temperature of weld pools by infrared two colour pyrometry," *Science and Technology of Welding and Joining*, vol. 15, no. 1, pp. 40–47, Jan. 2010, doi: 10.1179/136217109X12537145658814.
- [11] T. Font Comas, C. Diao, J. Ding, S. Williams, and Y. Zhao, "A Passive Imaging System for Geometry Measurement for the Plasma Arc Welding Process," *IEEE Transactions on Industrial Electronics*, vol. 64, no. 9, pp. 7201–7209, Sep. 2017, doi: 10.1109/TIE.2017.2686349.
- [12] P. K. Baghel and D. S. Nagesh, "INFLUENCING AND ANALYSIS OF TIG WELDING PROCESS ON MECHANICAL PROPERTIES OF EXTRUDED ALUMINUM PARTS," *Transactions of the Canadian Society for Mechanical Engineering*, vol. 41, no. 4, pp. 499–515, Nov. 2017, doi: 10.1139/TCSME-2017-1035.
- [13] W. Yiquan, W. Hong, Y. Zhilong, and G. Tie, "Noise reduction of welding defect image based on NSCT and anisotropic diffusion," *Transactions of Tianjin University 2014 20:1*, vol. 20, no. 1, pp. 60–65, Feb. 2014, doi: 10.1007/S12209-014-2124-Y.
- [14] F. Z. Boudani and N. Nacereddine, "Diffusion in the Wavelet Domain for Denoising Radiographic Images of Welding Defects," 2019 International Conference on Advanced Electrical Engineering, ICAEE 2019, Nov. 2019, doi: 10.1109/ICAEE47123.2019.9015093.
- [15] Y. Zou, X. Wei, and J. Chen, "Conditional generative adversarial network-based training image inpainting for laser vision seam tracking," *Optics* and Lasers in Engineering, vol. 134, p. 106140, Nov. 2020, doi: 10.1016/J.OPTLASENG.2020.106140.

- [16] C. LI, Q. WANG, W. JIAO, M. JOHNSON, and Y. M. ZHANG, "Deep Learning-Based Detection of Penetration from Weld Pool Reflection Images," Welding Journal, vol. 99, no. 9, pp. 239s–245s, Sep. 2020, doi: 10.29391/2020.99.022.
- [17] J. Stavridis, A. Papacharalampopoulos, and P. Stavropoulos, "Quality assessment in laser welding: a critical review," *International Journal of Advanced Manufacturing Technology*, vol. 94, no. 5–8, pp. 1825–1847, Feb. 2018, doi: 10.1007/S00170-017-0461-4.
- [18] F. Bouzaraa, "High Dynamic Range Imaging Systems for Dynamic Scenes".
- [19] S. Hajisharif, "Computational Photography: High Dynamic Rangeand Light Fields," vol. 2046, Feb. 2020, doi: 10.3384/DISS.DIVA-163693.
- [20] D. Bacioiu, G. Melton, M. Papaelias, and R. Shaw, "Automated defect classification of Aluminium 5083 TIG welding using HDR camera and neural networks," *Journal of Manufacturing Processes*, vol. 45, pp. 603–613, Sep. 2019, doi: 10.1016/J.JMAPRO.2019.07.020.
- [21] B. Zhang, Y. Shi, Y. Cui, Z. Wang, and X. Chen, "A high-dynamic-range visual sensing method for feature extraction of welding pool based on adaptive image fusion," *International Journal of Advanced Manufacturing Technology*, vol. 117, no. 5–6, pp. 1675–1687, Nov. 2021, doi: 10.1007/S00170-021-07812-X.
- [22] J. S. Chen, J. Chen, K. Zhang, Z. Feng, and Y. M. Zhang, "Dynamic reflection behaviors of weld pool surface in pulsed GTAW," *Welding Journal*, vol. 97, no. 6, pp. 191s–206s, Jun. 2018, doi: 10.29391/2018.97.017.
- [23] "VGG16 Convolutional Network for Classification and Detection." https://neurohive.io/en/popular-networks/vgg16/ (accessed Jul. 27, 2021).
- [24] K. He, X. Zhang, S. Ren, and J. Sun, "Deep Residual Learning for Image Recognition," *Proceedings of the IEEE Computer Society Conference on Computer Vision and Pattern Recognition*, vol. 2016-December, pp. 770–778, Dec. 2015, Accessed: Jul. 27, 2021. [Online]. Available: https://arxiv.org/abs/1512.03385v1
- [25] K. He, X. Zhang, S. Ren, and J. Sun, "Deep Residual Learning for Image Recognition," in *cvpr*, 2016, pp. 770–778. Accessed: Nov. 12, 2020. [Online]. Available: http://imagenet.org/challenges/LSVRC/2015/
- [26] C. Knaak, L. Masseling, E. Duong, P. Abels, and A. Gillner, "Improving Build Quality in Laser Powder Bed Fusion Using High Dynamic Range Imaging and Model-Based Reinforcement Learning," *IEEE Access*, vol. 9, pp. 55214–55231, 2021, doi: ·10.1109/ACCESS.2021.3067302.
- [27] R. Yu, J. Kershaw, P. Wang, and Y. M. Zhang, "Real-time recognition of arc weld pool using image segmentation network," *Journal of Manufacturing*

- *Processes*, vol. 72, pp. 159–167, Dec. 2021, doi: 10.1016/J.JMAPRO.2021.10.019.
- [28] Y. Cheng, R. Yu, Q. Zhou, H. Chen, W. Yuan, and Y. M. Zhang, "Real-time sensing of gas metal arc welding process A literature review and analysis," *Journal of Manufacturing Processes*, vol. 70, pp. 452–469, Oct. 2021, doi: 10.1016/J.JMAPRO.2021.08.058.
- [29] Y. Cheng *et al.*, "Detecting dynamic development of weld pool using machine learning from innovative composite images for adaptive welding," *Journal of Manufacturing Processes*, vol. 56, pp. 908–915, Aug. 2020, doi: 10.1016/J.JMAPRO.2020.04.059.
- [30] Q. Wang, W. Jiao, P. Wang, and Y. M. Zhang, "A tutorial on deep learning-based data analytics in manufacturing through a welding case study," *Journal of Manufacturing Processes*, vol. 63, pp. 2–13, Mar. 2021, doi: 10.1016/J.JMAPRO.2020.04.044.
- [31] W. Jiao, Q. Wang, Y. Cheng, and Y. M. Zhang, "End-to-end prediction of weld penetration: A deep learning and transfer learning based method," *Journal of Manufacturing Processes*, vol. 63, pp. 191–197, Mar. 2021, doi: 10.1016/J.JMAPRO.2020.01.044.
- [32] J. Kershaw, R. Yu, Y. M. Zhang, and P. Wang, "Hybrid machine learning-enabled adaptive welding speed control," *Journal of Manufacturing Processes*, vol. 71, pp. 374–383, Nov. 2021, doi: 10.1016/J.JMAPRO.2021.09.023.